Magnetization steps in $[Fe(salen)Cl]_2$

Y. Shapira and M. T. Liu
Department of Physics and Astronomy, Tufts University, Medford, Massachusetts 02155

S. Foner
Francis Bitter Magnet Laboratory, Massachusetts Institute of Technology, Cambridge, Massachusetts 02139

C. E. Dubé and P. J. Bonitatebus, Jr.
Department of Chemistry, Merkert Chemistry Center, Boston College, Chestnut Hill, Massachusetts 02167

(Received 14 May 1998)

The differential susceptibility dM/dH of $[Fe(salen)Cl]_2$ where salen is *N*,*N*′-ethylenebis(salicylideneiminato), was measured in pulsed magnetic fields up to 550 kOe. The samples were in a capsule that was immersed in a liquid-helium bath maintained at a temperature $1.5 \leqslant T_{bath} \leqslant 4.2$ K. Three magnetization steps (MST's) arising from energy-level crossings for the Fe^{3+} dimer were observed as peaks in dM/dH. The intradimer exchange constant obtained from the MST's is $J = -8.4 \pm 0.2$ cm^{-1}, assuming a g factor of 2.00. The line shapes of the peaks in dM/dH strongly suggest the existence of weak interactions that are not included in the conventional model of independent dimers with isotropic intradimer exchange only. The missing weak interactions are yet to be identified. The narrow widths of the peaks in dM/dH indicate strong departures from thermal equilibrium with the helium bath during the field pulse (milliseconds duration). Such narrow widths are the result of cooling by the magnetocaloric effect. The cooling, and therefore the line shapes of the dM/dH peaks, depended on the arrangement for the sample-to-bath heat flow during the field pulse. With one heat-flow arrangement hysteresis was observed. Computer simulations of the line shape resulting from the magnetocaloric effect during the field pulse reproduce the narrow widths and the hysteresis. Data for the low-field magnetic susceptibility between 2 and 300 K, measured in steady fields, gave $J \cong -8$ cm^{-1}. [S0163-1829(99)08101-1]

I. INTRODUCTION

Magnetization-step spectroscopy is a modern direct method of determining exchange interactions in transition-metal complexes. Many crystals contain polynuclear transition-metal complexes that are magnetically well isolated from each other. The magnetic behavior is then well approximated by a model of independent complexes, with magnetic interactions restricted to be within each complex. Much of our understanding of these intramolecular interactions comes from studies of dimers (binuclear complexes) and trimers (trinuclear complexes), although higher-nuclearity clusters have also been investigated.[1–5]

The exchange interaction is often the largest intramolecular magnetic interaction. The traditional experimental tool for determining the exchange constant(s) J has been the temperature variation of magnetic susceptibility χ. More advanced experimental methods of determining J include inelastic-neutron scattering,[6,7] and magnetization steps.[8–13] The last two techniques probe directly the energy-level structure. Besides yielding J, these two methods may reveal the presence of weak interactions in addition to the intramolecular-exchange interactions.

The magnetization-step (MST) method of determining exchange constants was developed in the context of dilute magnetic semiconductors, such as $Cd_{1-x}Mn_xTe$.[8–11] These materials contain a variety of ''magnetic clusters'' that are analogous to various polynuclear complexes of different nuclearity. Most of the early MST studies focused on the dimers, known as ''pairs'' in this context.

Thus far, the application of the MST method to polynuclear transition-metal complexes has been rather limited.[3,12,13] One reason is that the MST method is relatively new. More importantly, the method has some limitations. Exchange interactions give rise to MST's only when the interactions are antiferromagnetic (AF). In addition, the exchange constants cannot be too large if the MST's are to be observed with available magnetic fields. For example, even with fields as high as 600 kOe, $|J|$ must be less than about 30 cm^{-1} for a typical g factor of 2. In many molecules, the magnitude of J is larger. The choice of $[Fe(salen)Cl]_2$ for the present MST study was partially motivated by its unusually weak AF exchange.

The crystal structure of $[Fe(salen)Cl]_2$ was determined by Gerloch and Mabbs.[14] The two Fe^{3+} ions in the dimer occupy equivalent sites, separated by 3.29 Å. These Fe^{3+} ions are bridged by a pair of oxygen atoms. The Fe-O-Fe bond angle is about 90°. The spin of the Fe^{3+} ion is $\frac{5}{2}$. Because it is an S state ion, the g factor is expected to be close to 2.00, and anisotropic interactions in the dimer are expected to be very weak. The conventional model for the magnetic properties of $[Fe(salen)Cl]_2$ is therefore of independent dimers with isotropic intradimer exchange interaction and no anisotropy. There have been several determinations of the exchange constant J for this dimer. Early susceptibility data[15,16] gave $J \cong -7.5$ cm^{-1}. A later study of the hyperfine interactions, using the Mössbauer effect,[17] gave $J = -7.0$ cm^{-1}.

II. THE MAGNETIZATION-STEPS METHOD

MST's arise from many types of transition-metal complexes, among which the dimer is the simplest. Here, we

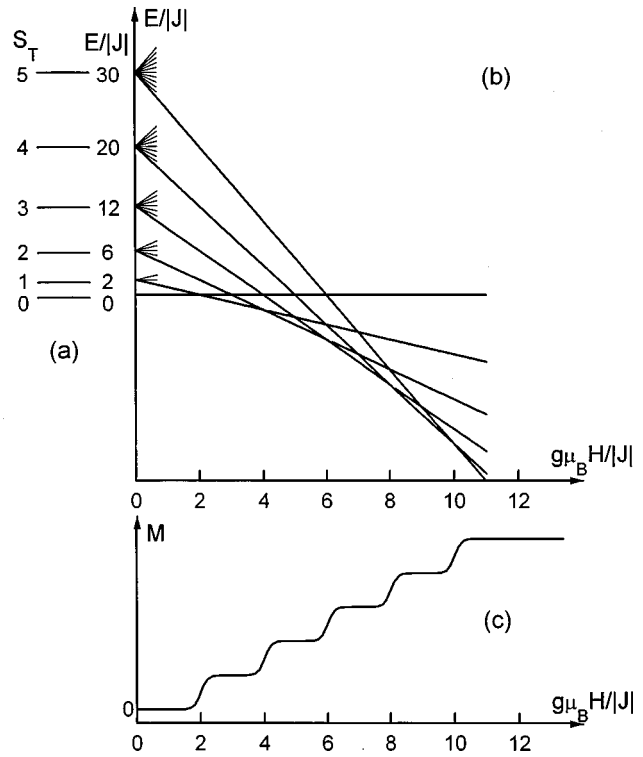

FIG. 1. (a) Energy levels for a dimer at zero magnetic field. The energy E depends on the magnitude of the total spin S_T. The ground-state energy is taken as zero. (b) Zeeman splitting of the dimer's energy levels. Note the changes in the ground state, due to level crossings. (c) The dimer magnetization at low temperatures.

briefly review the physics of MST's arising from dimers composed of two identical ions, each with spin S. The dimers are assumed to be independent of each other. The intradimer exchange interaction has the form $-2J\mathbf{S}_1\cdot\mathbf{S}_2$. All anisotropic interactions are ignored.

The energy levels of a dimer in a magnetic field **H** are given by

$$E=-J[S_T(S_T+1)-2S(S+1)]+g\mu_B mH, \qquad (1)$$

where S_T is the magnitude of the total spin of the dimer, which can vary between zero and $2S$, m is the component of the total spin along **H**, and μ_B is the Bohr magneton. Figure 1(a) shows the energy levels at $H=0$ when the exchange interaction is AF. The Zeeman splitting of these levels is shown in Fig. 1(b). The crucial point is that there is a series of level crossings at which the ground state changes. In increasing H, each of these level crossings raises the value of $|m|$ in the ground state by one unit. If the temperature is low enough ($k_BT<|J|$, where k_B is the Boltzmann constant) then this change of $|m|$ leads to a step in the magnetization M. The series of MST's is shown in Fig. 1(c). The magnetization change ΔM at each of the MST's is the same. The level crossings, and hence the MST's, occur at fields H_n which are given by

$$g\mu_B H_n=2|J|n, \qquad (2)$$

where $n=1,2,\ldots,2S$. For a dimer composed of Fe^{3+} ions there are therefore five MST's. If any of these MST's is observed, then J can be obtained from the measured H_n using Eq. (2) and the known, or assumed, value of g.

Each MST is associated with a peak in the differential susceptibility dM/dH. The line shape of the peak can be obtained from the known analytic expression for the magnetization of dimers.[18] Under isothermal conditions, the peak in dM/dH is symmetric, and its width δH at half height is proportional to the temperature T,

$$g\mu_B\delta H=3.53k_BT. \qquad (3)$$

The isothermal line shape can change, and the width can increase, when interactions other than the isotropic intradimer exchange are included.[8] However, much more drastic changes in the line shape can occur when the experiments are performed in pulsed magnetic fields of milliseconds duration. Thermal equilibrium may not prevail during such a short pulse. The temperature of the spin system may then vary appreciably during the measurement, which will have a strong effect on the line shape.[19,20] These magnetocaloric effects will be considered later when the experimental line shapes are discussed.

III. EXPERIMENT

A. Materials

Salicaldehyde, 1,2-diaminoethane, anhydrous ethanol, and $FeCl_3$ were purchased from Aldrich and used as received. The ligand H_2salen [N,N'-bis(salicylidene)-1,2 diaminoethane] was synthesized by reaction of two equivalents of salicaldehyde with one equivalent of 1,2-diaminoethane, and the resulting product was recrystallized from ethanol. The preparation of $[Fe(salen)Cl]_2$ followed Ref. 14, and was performed under prepurified argon using standard drybox techniques. Four samples (*B, C, D,* and *E*) were recrystallized from acetone under ambient conditions. The fifth sample (*A*) was recrystallized by diffusion of diethyl ether into an acetone solution of $[Fe(salen)Cl]_2$ at 4 °C. Elemental analyses on each of the five samples showed good agreement with each other. The values (in wt %) calculated from the chemical formula $Fe_2C_{32}H_{28}N_4O_4Cl_2$ are as follows: Fe, 15.62; C, 53.73; H, 3.95; N, 7.83. The average values actually found in the five samples were as follows: Fe, 15.62; C, 53.27; H, 3.88; N, 7.69. The elemental analyses were obtained from Desert Analytics, Tucson, AZ.

X-ray measurements were made on a red-brown needle from sample *B*. These data were taken at 183 K with Mo $K\alpha$ radiation ($\lambda=0.71073$ Å) using a Siemens SMART charge-coupled device (CCD) area-detector diffractometer.[21] The results [space group $P2_1/c$, and unit cell parameters $a=11.336(4)$ Å, $b=6.884(2)$ Å, $c=19.172(6)$ Å, $\beta=91.26(2)°$] are in good agreement with literature values.[14]

B. Differential susceptibility in pulsed fields

The experimental arrangements for the pulsed field experiments are described elsewhere.[9] The data were obtained with a 1.27-cm bore liquid-nitrogen-cooled magnet. Magnetic fields up to 450 or 550 kOe were used. The shape of the field pulse was approximately a half cycle of a weakly damped sine wave with a half period of 7.4 ms (3.1 ms field rise time, and 4.3 ms fall time).

A small liquid He Dewar with a 1.02 cm o.d. and 0.635 cm i.d. tail section, made with 0.5 mm precision bore glass tubing, contained a well-balanced set of detection coils. This coil system, positioned at the center of the pulsed magnet, detected the time derivative of the magnetization dM/dt of the sample during the pulse. The temperature of the He bath was fixed between 4.2 and 1.5 K. As noted later, during the pulse there was a large difference between the bath and sample temperatures, due to magnetocaloric effects.

The sample, 10–15 mg of finely ground powder, was placed in a thin-walled (0.25 mm) cylindrical capsule made of Delrin. In most experiments, the capsule had a small hole at the bottom, allowing liquid helium to enter the sample space. However, in one set of experiments there was no hole at the bottom, and the capsule was sealed at the top with a tight-fitting silicone-greased phenolic rod. The purpose of removing the hole was to prevent liquid helium from entering the sample space, thereby limiting the heat flow to and from the sample during the field pulse. Judged by the results, there was no significant sample-to-bath heat flow during the milliseconds field pulse in this case.

The sample was positioned in the detection pickup coils. After each run the sample was moved out of the pickup coils while they remained in place, and the small background unbalanced signal from the field pulse was measured. The corrected dM/dt signal was obtained by subtracting the background digitally. The dH/dt signal was obtained during the pulse from an independent pickup coil wound on the outside of the Dewar tail. The dM/dt and dH/dt signals, both as a function of t, were recorded simultaneously using multichannel data acquisition. The (corrected) dM/dt signal was converted to dM/dH by using the dH/dt signal. The field $H(t)$ was obtained by integrating dH/dt. The final result was for the differential susceptibility dM/dH versus H. It should be noted that measurements of dM/dt can detect very small changes in M if the changes take place in a short time.

C. Susceptibility measurements

The magnetic susceptibility was measured using a superconducting quantum interference device (SQUID) magnetometer system manufactured by Quantum Design Inc. The system, which uses steady magnetic fields, was operated in temperatures $2 \leqslant T \leqslant 300$ K. The susceptibility as a function of T was measured in fields of 1 or 3 kOe. Isothermal magnetization curves in fields up to 55 kOe were also obtained at several temperatures.

IV. MAGNETIZATION STEPS

A. Exchange constant J from MST's

The differential susceptibility dM/dH of samples *A, B, D,* and *E* was measured in pulsed fields. Each sample consisted of many unoriented crystallites. Most data were taken in fields up to 450 kOe, but some measurements extended up to 550 kOe. The capsule containing each of the samples was in a helium bath. The bath temperature T_{bath} was usually 1.5 K, but some additional data with T_{bath} up to 4.2 K were also obtained.

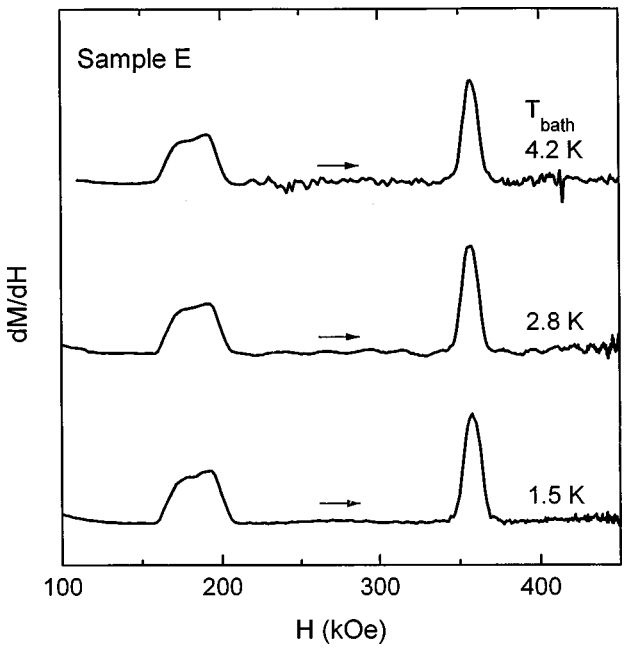

FIG. 2. Differential susceptibility dM/dH of sample *E* in pulsed fields. These data are for increasing H. Curves obtained at different helium-bath temperatures T_{bath} are displaced vertically relative to each other, but the vertical gain is the same. For this sample there was no hole in the capsule containing the sample, so that the flow of liquid helium into the capsule was prevented.

As noted, two arrangements for the sample-to-bath heat flow were used. For samples *A, B,* and *D,* a hole in the capsule provided a direct contact between the sample and the helium bath. The pulsed field data for these three samples were remarkably similar. In the case of sample *E,* there was no hole. The data for this sample indicate that adiabatic conditions prevailed during the milliseconds field pulse. The simulations described in Sec. IV B 3 assume that even when there was no hole, the much longer time interval between pulses (at least 10 min) allowed the sample to reach equilibrium with the bath.

Figure 2 shows data for sample *E* at $T_{\text{bath}} = 1.5$, 2.8, and 4.2 K. These data are for increasing H. The two peaks near 180 and 360 kOe correspond to the first two MST's ($n = 1,2$) from the dimer. The centers of the two peaks were identified as the fields H_1 and H_2 where the ground state changes due to level crossings. As expected, these fields do not depend on T_{bath}. The same values for H_1 and H_2 were also obtained by integrating the dM/dH data and locating the midpoint of the rise in the magnetization M. The dM/dH data for decreasing H were similar, and gave nearly the same values for H_1 and H_2. The overall average values for this sample were $H_1 = 181$ kOe and $H_2 = 357$ kOe. The ratio $H_2/H_1 = 1.97$ is close to the value 2.00 predicted by Eq. (2). These results for H_1 and H_2 lead to an intradimer exchange constant $J = -8.4\ \text{cm}^{-1}$, assuming a g factor of 2.00 for the Fe^{3+} ion.

The line shapes in Fig. 2 exhibit some unusual features: (1) the dM/dH peak associated with the first MST is much wider than the second, and (2) the widths of the peaks indi-

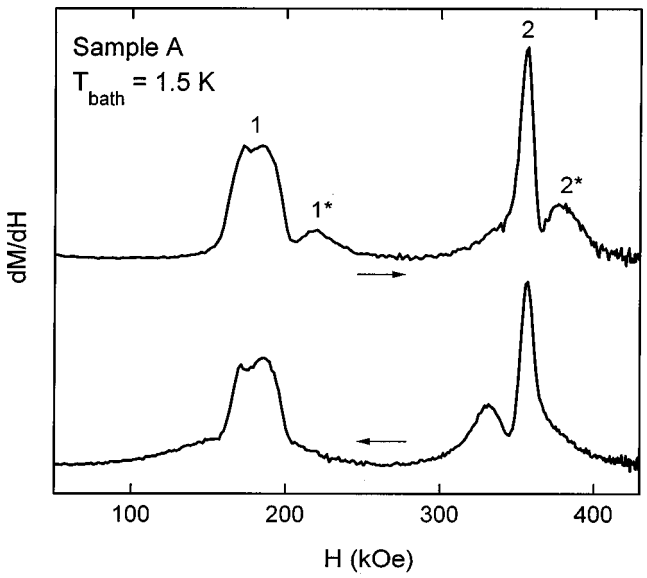

FIG. 3. Differential susceptibility dM/dH of sample *A* in pulsed fields. The curves for the up and down portions of the field pulse are displaced vertically relative to each other. A hole in the capsule containing the sample allowed liquid helium to make contact with the sample.

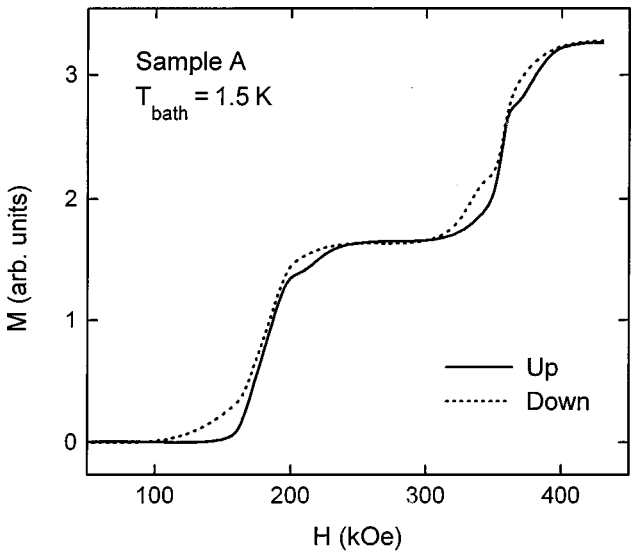

FIG. 4. Magnetization curve for sample *A*, obtained by integrating the data in Fig. 3. The solid and dashed curves are for the up and down portions of the field pulse, respectively.

cate strong departures from thermal equilibrium with the helium bath. These features, which do not affect the value of *J*, will be discussed later.

Figure 3 shows an example of dM/dH data taken with a hole in the capsule. The upper curve is for increasing fields (''up'' portion of the pulse), while the lower curve is for decreasing fields (''down'' portion). There are many similarities but also some striking differences between the up and down traces. There are also similarities and differences between either of these traces and those in Fig. 2, which were obtained with no hole in the capsule. In both Figs. 2 and 3 there are two main peaks, labeled as 1 and 2 in Fig. 3. Peak 2 is always narrower and taller than peak 1. The main new feature in Fig. 3, which does not exist in Fig. 2, is the appearance of the ''satellites'' 1* and 2* in addition to the main peaks 1 and 2.

The fields at the main peaks in Fig. 3 are nearly the same in the up and down traces, and they also agree with the fields H_1 and H_2 in Fig. 2. On the other hand, the fields at the satellites in Fig. 3 are very different in the up and down traces. In the up trace the fields at 1* and 2* are higher than those at 1 and 2, respectively. In the down trace, on the other hand, satellite 2* is at a lower field than peak 2, and only a vestige of satellite 1* is observed at fields below peak 1. It is noteworthy that as a function of *time* the satellites in both up and down traces of Fig. 3 always occur *after* the main peaks. The differences between the up and down results in Fig. 3 imply that thermodynamic equilibrium did not prevail during the pulse. The nonequilibrium effects exhibited by the data of Figs. 3 and 2 are discussed later.

Figure 4 shows the magnetization *M* obtained by integrating the dM/dH data in Fig. 3. There are two large MST's. As expected, the magnetization change ΔM associated with each step is the same for both steps. The hysteresis in each of the steps corresponds to the difference between the up and down results for dM/dH.

The values of H_1 and H_2 for the samples *A*, *B*, and *D* (which exhibited satellites) were determined from *M* vs *H* curves such as Fig. 4. For each MST there is a field where the change in *M* is equal to half of the total change ΔM associated with that MST. This field, at the midpoint of the magnetization rise, was chosen as H_n. The values of H_1 and H_2 obtained in this manner were very close to the centers of the main peaks 1 and 2 in the corresponding dM/dH traces. The values of H_1 and H_2 were also nearly the same for increasing and decreasing *H*.

The exchange constant $J=-(8.4\pm0.2)$ cm^{-1} was obtained from the results for H_1 and H_2 in all four samples which were measured in the pulsed fields. All up and down traces were included, and *J* was calculated from Eq. (2) assuming $g=2.00$. The uncertainty is mainly due to a scatter in values of H_1 and H_2.

Most of the measurements were in fields up to 450 kOe, and they revealed only two MST's. However, pulses up to 545 kOe were also used for sample *D* (with hole in the capsule) and for sample *E* (no hole). These traces uncovered a sizable portion of the third MST. Figure 5 shows the magnetization curve obtained by integrating the dM/dH data in the up trace for sample *D*. For both samples *D* and *E* the estimated experimental values for H_3 were somewhat lower than expected from the values of H_1 and H_2. The values for H_3 gave $J\cong-8.2$ cm^{-1}.

B. Line shapes

1. General features

In the conventional model (CM) for [Fe (salen)Cl]$_2$ the dimers are independent of each other, and the only magnetic interaction is the intradimer isotropic exchange. One conclusion from the analysis of the line shapes of the dM/dH peaks is that there are also other magnetic interactions, although much weaker than the isotropic intradimer exchange. The line shapes in pulsed fields also exhibit spectacular mag-

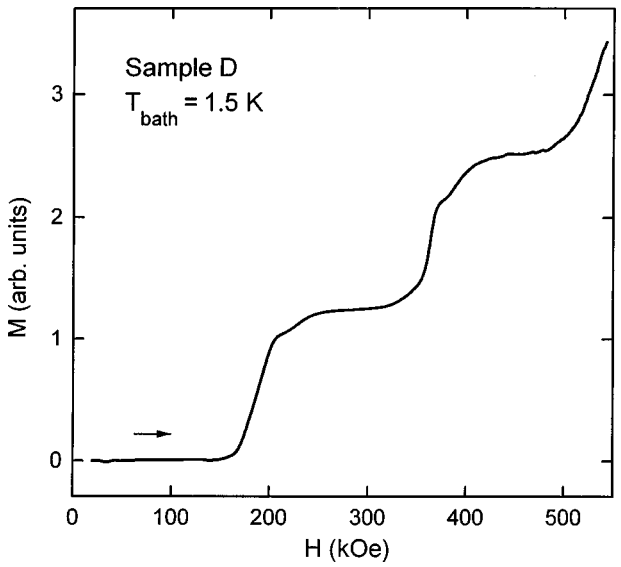

FIG. 5. Magnetization curve for sample *D* (with hole in capsule), obtained by integrating data for dM/dH. These results are for the up portion of the field pulse.

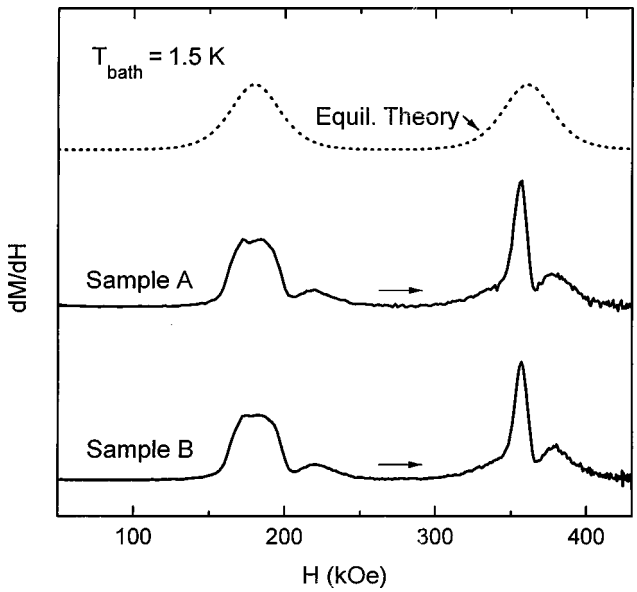

FIG. 6. Measured dM/dH traces for samples *A* and *B* in the up portion of the field pulse (solid lines). These results were obtained with a hole in the capsule. The trace for sample *A* is the same as the up trace in Fig. 3. The equilibrium simulation (dashed curve) was calculated assuming thermal equilibrium with the helium bath, and the conventional model for the magnetic intractions. All curves are for $T_{\text{bath}}=1.5$ K.

netocaloric effects. As each MST is approached, the sample's temperature drops dramatically.

The line shapes expected from the CM and the assumption of thermal equilibrium with the helium bath are illustrated by the dashed curve in Fig. 6. The equilibrium shapes of the two peaks near 180 and 360 kOe are identical. Both peaks are symmetric, and neither exhibits a structure or a satellite. The linewidth is purely thermal in origin and is given by Eq. (3).

The temperature T, which should be used in Eq. (3) is the spin temperature T_s. In the equilibrium simulation shown in Fig. 6, T_s was set equal to $T_{\text{bath}}=1.5$ K. The calculated thermal width (full width at half height) of the dM/dH peak at this temperature is then 39 kOe. The calculated thermal width at 4.2 K is 110 kOe. In contrast, the observed second peak in Fig. 2 (measured with no hole in the capsule) is only 12 kOe wide at all bath temperatures between 1.5 and 4.2 K. Clearly, the actual spin temperature T_s at the second peak is substantially below T_{bath}. For the higher bath temperatures in Fig. 2, even the first peak is much narrower than the width calculated with $T_s=T_{\text{bath}}$. Thus, the first peak in Fig. 2 is also strongly affected by magnetocaloric effects.

The solid curves in Fig. 6 are examples of data obtained with a hole in the capsule. There are striking differences between either experimental curve and the equilibrium simulation (dashed curve). These differences include (1) the existence of satellites; (2) the observed main peak near 360 kOe has a width of 10 kOe compared to the 39 kOe equilibrium thermal width; (3) the first main peak, near 180 kOe, is much broader than the second peak, and it shows a structure which is not fully resolved. The structure is not peculiar to up traces, as illustrated by the down trace in Fig. 3. Figure 2 shows that the structure in the first peak also appears when there is no hole in the capsule. The differences between the observed line shapes and those in the equilibrium simulation are attributed to magnetocaloric effects, and to weak magnetic interactions which are not included in the CM.

2. Evidence for additional interactions

Evidence for weak interactions, in addition to the dominant isotropic intradimer exchange, comes largely from the structure of the first dM/dH peak, near 180 kOe. It is unlikely that this structure is the result of magnetocaloric effects because it does not appear in the simulations of these effects (discussed below). In addition, Fig. 2 shows that the structure is independent of the bath temperature, up to 4.2 K, suggesting that it is intrinsic and is not thermal in origin. The most probable interpretation is that in addition to the intradimer exchange there are weaker interactions, which are responsible for the structure. One known weak interaction is the magnetic dipole-dipole interaction within the dimer. However, the dipole-dipole interaction is too weak to explain the structure. Other possibilities are weak interactions between different dimers, or some weak intradimer anisotropy. The identity of the missing weak interaction(s) is unknown.

The most puzzling experimental result is that the second dM/dH peak, near 360 kOe, does not show the structure exhibited by the first peak. The reason for the difference is unknown. The fact that the second peak is much narrower does not mean, however, that its width can be accounted for by the CM, which includes only the intradimer isotropic exchange. The width of the second peak in Fig. 2 does not change with T_{bath}, strongly suggesting that this width also is largely intrinsic rather than thermal. In the CM, with isotropic intradimer exchange only, the width is entirely thermal. Any nonthermal width must result from additional interactions. Later, in the simulations of the magnetocaloric effects, an additional term will be added formally to the Hamiltonian in order to account for the intrinsic width of the second peak.

3. Magnetocaloric effects

As noted, the widths of the MST's in Fig. 2 are narrower, by a factor up to 9, than the thermal widths calculated using

the helium-bath temperature T_{bath}. In addition, the line shapes in Figs. 3 and 2 are very different, reflecting the different sample-to-bath thermal contact when there is and there is not a hole in the capsule. These are manifestations of strong magnetocaloric effects during the field pulse. A discussion and computer simulations of these effects are presented below.

To maintain the spin system at a constant temperature while H is changing rapidly requires a rapid heat transfer to and from the spin system. There are several steps in this heat transfer. First, heat must be exchanged between the spins and the lattice, which involves the spin-lattice relaxation. However, at temperatures below 4.2 K even a rapid spin-lattice relaxation will fail to maintain the spin system at a constant temperature during the field pulse. The reason is that the lattice specific heat is expected to be small compared to the magnetic specific heat of the dimers near the MST's. Therefore, the lattice cannot act as a constant temperature reservoir. The temperature T_s of the spin system will remain equal to the T_{bath} only if heat can also be exchanged rapidly between the lattice and the bath.

If the heat flow between the lattice and the bath is not sufficiently rapid (so-called ''phonon bottleneck''), T_s will vary significantly during the field pulse. Such magneotcaloric effects were discussed in Refs. 19 and 20. When each of the fields H_n is approached from either lower or higher fields, the spin system cools. As noted by Wolf long ago,[22] the cooling process near H_n is analogous to the familiar cooling by adiabatic demagnetization of a paramagnet. The main difference is that for an ideal paramagnet the ground level is degenerate at $H=0$, while for MST's in the CM the ground level is doubly degenerate at each H_n [Fig. 1(b)]. Thus, for a paramagnet the cooling occurs as H is reduced to zero, whereas for MST's the cooling occurs as H approaches any H_n.

The degree of cooling depends on several factors. Besides the lattice-bath thermal contact the cooling is limited by the minimum-energy separation between the two states responsible for the MST. In Fig. 1(b), which is based on the CM, the energy levels cross so that the minimum energy separation is zero. In reality, however, weak interactions, which are not included in the CM may result in an anticrossing, and hence in a finite minimum-energy separation.[8] The anticrossing leads to an intrinsic (nonthermal) width of the MST. The minimum-energy separation limits the lowest achievable temperature.[22] Although the weak interactions leading to an anticrossing in the present system have not been identified, such an anticrossing was assumed in the nonequilibrium simulations discussed below. Formally, the anticrossing was introduced by adding a small off-diagonal matrix element D connecting the two states responsible for the MST.[8]

The cooling that occurs as H_n is approached can be very large. In some of the simulations below, the lowest T_s is only a few percent of the initial temperature (equal to T_{bath}). After the field H sweeps through H_n, the spin system warms. Under adiabatic conditions (no lattice-to-bath heat transfer) the spin system warms gradually until it returns to the bath temperature. However, for a finite lattice-to-bath heat transfer, shortly after H passes through H_n the spin temperature T_s is actually higher than T_{bath}. In that case, as H moves further away from H_n the spin temperature gradually cools toward T_{bath}.[19]

The variation of T_s during the pulse changes the shape of the MST. Under adiabatic conditions the cooling near H_n leads to a much narrower MST, but the shape of the dM/dH peak remains symmetric. A more complicated line shape is obtained for a finite lattice-to-bath heat flow. The cooling as H approaches H_n leads to a faster magnetization change on the approaching side of the MST. The dM/dH peak on the approaching side is therefore narrower than it would have been had T_s remained equal to T_{bath}. The line shape on the receding side of the MST, after the field has passed through H_n, is sensitive to the warming that occurs in this field region. The computer simulations in Ref. 19 gave a single asymmetric dM/dH peak, which was narrow on the approaching side but broad on the receding side. This type of line shape is obtained only for a certain range of parameters. For another range of parameters, satellites appear.

The present computer simulations used the method in Ref. 19. A common temperature T_s for the spins and the lattice was assumed. The equation for the time rate of change of T_s is

$$\frac{dT_s}{dt} = -\frac{T_s}{C_H}\left(\frac{\partial M}{\partial T_s}\right)_H\left(\frac{dH}{dt}\right) + \frac{1}{C_H}\left(\frac{dQ}{dt}\right), \tag{4}$$

where C_H is the specific heat at constant H of the combined spin-lattice system, and dQ/dt is the rate of heat flow from the bath to the spin-lattice system. Under adiabatic conditions (no hole in the capsule) there is no heat flow. For a sample immersed in a helium bath (hole in the capsule) the heat flow was assumed to have the form

$$\frac{dQ}{dt} = C(T_{\text{bath}}^p - T_s^p), \tag{5}$$

where C is a constant. Most of the simulations were made with the value $p=4$ obtained by Khalatnikov.[23] With this p, Eq. (5) leads to the familiar $1/T^3$ dependence of the Kapitza thermal boundary resistance between liquid helium and a solid when the difference between T_{bath} and T_s is small.[24] The simulations were performed with a variety of values for the constant C. A zero value for C corresponds to adiabatic conditions.

The specific heat C_H contains a lattice contribution and a magnetic contribution from the dimers. The lattice specific heat was unknown, but was expected to be relatively unimportant. The actual simulations used the lattice specific heat from a Debye model with one atom per cell,[25] and with a Debye temperature $\Theta = 100$ K. (Simulations with Θ larger or smaller by a factor of three gave practically the same results for dM/dH. The reason is that in the relevant range of magnetic fields, C_H is dominated by the magnetic specific heat of the dimers.) The simulations included only the two dimer's energy levels responsible for the MST.

An off-diagonal matrix element $D = 0.3\ \text{cm}^{-1}$ was used in most simulations because this value leads to linewidths close to those observed for the peak near 360 kOe. Other values for D, down to $0.001\ \text{cm}^{-1}$, were also tried. The magnetization and specific heat of the dimers at given T_s and H were calculated using standard methods.[1–5] For simplicity, the

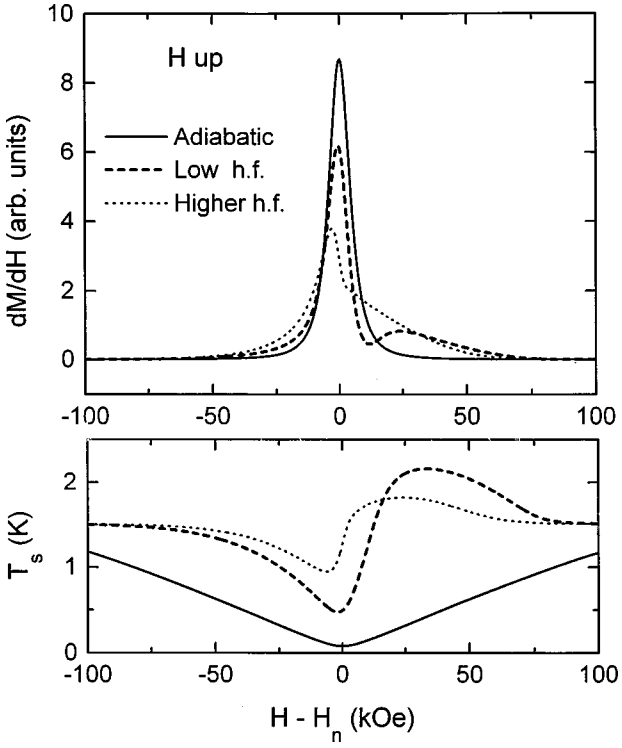

FIG. 7. Computer simulations for dM/dH and the spin temperature T_s when the sample is not in thermal equilibrium with the helium bath during the field pulse. The model is discussed in the text. Solid curves are for adiabatic conditions. The heavy dashed curves and the dotted curves are for two different rates of heat flow (h.f.) between the bath and the sample. All simulations are for $T_{\text{bath}}=1.5$ K, and are for the up portion of the field pulse.

time rate of change of the field dH/dt was assumed to be constant. Most simulations were for $T_{\text{bath}}=1.5$ K, but some were for higher T_{bath}.

Figure 7 shows examples of simulations with $D=0.3\ \text{cm}^{-1}$ and $T_{\text{bath}}=1.5$ K. Part (a) gives the shape of the dM/dH curve, and part (b) the variation of T_s. Both parts are only for the up portion of the field pulse. The solid curves are the simulations under adiabatic conditions. The other two sets of curves are for two different nonzero values of the heat-flow (h.f.) constant C.

The simulation of dM/dH under adiabatic conditions and with $T_{\text{bath}}=1.5$ K gives a good representation of the experimental data for the second peak in the lowest curve in Fig. 2. The width of the simulated peak (10 kOe) is much smaller than the thermal width at the bath temperature (39 kOe). The simulated peak is symmetric, and there are no satellites. Additional simulations for T_{bath} from 1.5 up to 4.2 K show that under adiabatic conditions the shape of the dM/dH peak is practically independent of T_{bath}. These results account for the insensitivity of the curves in Fig. 2 to a change of T_{bath}. For T_{bath} above 10 K, the simulations under adiabatic conditions show a significant dependence on T_{bath}. As T_{bath} increases the peak becomes wider and smaller. The results of the simulations under adiabatic simulations are the same for increasing and decreasing H.

Results of simulations for a finite sample-to-bath heat flow depend on the ratio $C/(dH/dt)$, which affects the rate of heat flow per unit field dQ/dH. (The heat-flow constant C and dH/dt do not enter separately into the results. In the present experiments $dH/dt\sim 10^8$ Oe/s). The thin-dotted and heavy-dashed curves in both parts of Fig. 7 represent results for two heat-flow rates. The thin-dotted curves are similar to those in Ref. 19. The asymmetric dM/dH peak in this case is narrow on the approaching side but is much wider on the receding side. This particular simulation was obtained with a value of $C/(dH/dt)$, which corresponds to $dQ/dH=400\ (\text{erg/mol Oe K}^4)\Delta T^4$ in the analog of Eq. (5). The very different line shape represented by the heavy-dashed curve in Fig. 7(a) is for a value of $C/(dH/dt)$, which is smaller by a factor of three. For this lower heat flow, the dM/dH curve shows a narrow main peak (width$\cong$10 kOe) on the approaching side, followed by a well-developed satellite on the receding side. These results give good account of the data in Figs. 3 and 6 (with hole in the capsule). Simulations for the down portion of the field pulse show that for decreasing H all the curves in Fig. 7 should be reflected about a vertical line at $H-H_n=0$. Thus, in decreasing fields the satellite will appear at fields lower than the main peak, i.e., as a function of time the satellite always follows the main peak. This result accounts for the main difference between the up and down traces in Fig. 3.

Additional simulations show that the satellite persists for a range of the heat flow rates, although the size and position of the satellite change with $C/(dH/dt)$. The value 4 for the exponent p in Eq. (5) is not critical for obtaining a satellite. Satellites were also obtained in simulations with $p=1$, 2, 3, and 5. Other forms for the heat-flow also lead to a satellite. For example, a satellite is obtained when Eq. (5) is replaced by

$$\frac{dQ}{dt}=C^*T_s^3(T_{\text{bath}}-T_s), \tag{6}$$

provided that the constant C^* is within a certain range.

The satellite persisted when the off-diagonal matrix element D was reduced gradually from 0.3 to 0.001 cm^{-1}. Thus, the appearance of a satellite is not restricted to a narrow range of D. However, the ratio between the size of the satellite and the main peak in dM/dH is parameter dependent. As already noted, most simulations were made with $D=0.3\ \text{cm}^{-1}$ because this value corresponds to the observed (intrinsic) width of the second peak in Fig. 2. The satellite is substantially smaller in simulations with $D=0.01\ \text{cm}^{-1}$, even when the heat flow is adjusted to maximize the satellite. For $D=0.001\ \text{cm}^{-1}$ the satellite is smaller still.

Physically, the satellite is a consequence of the warming that occurs after H passes through H_n. The fast rise of T_s temporarily arrests, or slows down substantially, the rapid population redistribution between the two energy levels that are involved. With some parameters the direction of the population redistribution may even be reversed for a short period of time. Thus, the change in the magnetization, which is a consequence of the population redistribution, is slowed down, or stops, or is even reversed, for a short period of time. The derivative dM/dH then drops temporarily. The satellite (new peak in dM/dH) appears when the rapid population redistribution resumes due to the increasing energy

splitting between the two levels. Once all the population is in the new lower energy level, the change in the magnetization is complete.

V. SUSCEPTIBILITY

Susceptibility data were taken on samples *A*, *B*, and *C*, each consisting of many unoriented crystallites. Data in fields of 1 and 3 kOe were taken in the following temperature ranges: 2–300 K for sample *A*, 2–280 K for sample *B*, and 2–100 K for sample *C*. Three small corrections were applied to the raw data: (1) a correction for the addenda, consisting of a plastic capsule and some Mylar tape; (2) a correction for the diamagnetic susceptibility of the lattice, $\chi_d = -4.87\times10^{-7}$ cm^3/g (Ref. 26); (3) a correction for a small concentration of paramagnetic ions, as discussed below.

For temperatures $k_BT \ll |J|$ nearly all the Fe^{3+} dimers should be in the ground state, with a zero net spin. The dimers' susceptibility should then be very small, and it should decrease with decreasing *T*. The need for the third correction became apparent when the measured susceptibility at $T \leqslant 4$ K (after the addenda and diamagnetic corrections) did not follow these predictions. First, the susceptibility χ was much higher than expected for the Fe^{3+} dimers. Second, χ increased on cooling from 4 to 2 K. Finally, the magnetization curve at 2 K, measured in steady magnetic fields up to 55 kOe, was inconsistent with Fe^{3+} dimers. This curve, *M* versus *H*, was concave down and the magnetization showed a tendency to saturate. For Fe^{3+} dimers the magnetization curve below 55 kOe should be concave up, and it should not show a tendency to saturate. In addition, the magnitude of *M* was much higher than expected for the dimers.

The unexpected behavior at $T \leqslant 4$ K was attributed to a small concentration of paramagnetic ions. The alternative possibility is that the CM for the magnetic behavior of $[Fe(salen)Cl]_2$ is oversimplified, and the unexpected behavior is intrinsic to the material. Intrinsic behavior, however, should be the same for all three samples, which was not the case. The deviations from the expected behavior were much larger for sample *C* than for samples *A* and *B*. For this reason the deviations were attributed to a small concentration of paramagnetic ions. It is noteworthy that to detect a small concentration of paramagnetic ions the susceptibility must be measured at temperatures $k_BT \ll |J|$ where the dimers' contribution is very small. The early susceptibility data[15,16] were all taken at $k_BT > 1.8|J|$. In the present work, the lowest *T* corresponded to $0.17|J|$.

The existence of a small concentration of paramagnetic ions is not surprising given that a monomeric form of [Fe(salen)Cl] also exists.[15] It is also possible that some other paramagnetic ions were present due to impurities. Regardless of the origin of the paramagnetic ions, at 2 K their magnetic moment should saturate in fields well below the beginning of the first MST from the Fe^{3+} dimers (centered near 180 kOe). The saturation moment of the paramagnetic ions M_{para} was therefore determined from the 2 K magnetization data to 55 kOe. The fits used to determine M_{para} are discussed below. For sample *A*, M_{para} was only 0.2% of the calculated saturation moment of the Fe^{3+} dimers. The corresponding values for samples *B* and *C* were 0.3% and 1.0%, respectively.

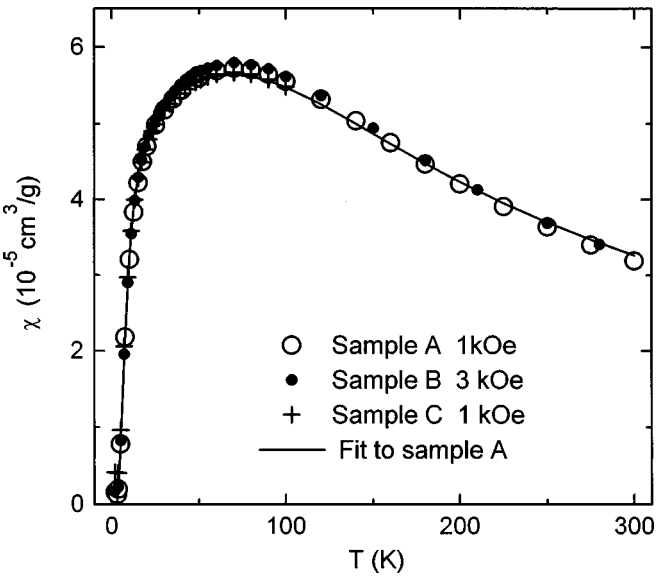

FIG. 8. Comparison between susceptibility data for the three samples. These results include all three corrections: addenda, diamagnetism, and paramagnetic ions. The solid curve is a fit of the corrected data for sample *A* to the theoretical susceptibility of dimers in the CM, with $J = -8.33$ cm^{-1} and $g = 2.037$.

To isolate the susceptibility of the dimers, it was necessary to correct for the contribution of the paramagnetic ions. The correction method assumed that the paramagnetic ions were Fe^{3+} ($S = \frac{5}{2}$, $g = 2.00$), and that their magnetization at 2 K followed the modified Brillouin function introduced by Gaj, Planel, and Fishman.[27] In the modified Brillouin function the actual temperature is replaced by an effective temperature $(T + T_0)$. The two parameters of the function, M_{para} and T_0, were obtained from fits to the magnetization data at 2 K. The values for M_{para} were already quoted. The values for T_0 were near 3 K for samples *A* and *B*, and near 1.5 K for sample *C*. The same modified Brillouin function was then used to calculate the low-field susceptibility of the paramagnetic ions at all temperatures. This approach is equivalent to using the Curie-Weiss law, with $\Theta = -T_0$.

Figure 8 shows results for the dimers' susceptibility in all three samples, after all the corrections (addenda, lattice diamagnetism, and paramagnetic ions) were made. The exchange constant *J* was obtained by fitting the corrected susceptibility data, $\chi(T)$, to the standard expression for the susceptibility of dimers in the CM.[1–5] This expression contains two parameters, *J* and the *g* factor. In some fits *g* was held fixed at 2.00, while in others it was allowed to vary. Fits which assumed $g = 2.00$ gave $J = -8.1$, -8.0, and -8.1 cm^{-1} for samples *A*, *B*, and *C*, respectively. The statistical uncertainties were less than 0.1 cm^{-1}. The value for sample *C* was judged to be somewhat less reliable because of the larger correction for paramagnetic ions, and the more limited temperature range. When the *g* factor also was allowed to vary in the fit, the results were $J = -8.3$ cm^{-1} and $g = 2.04$ for sample *A*, and $J = -8.3$ cm^{-1} and $g = 2.05$ for sample *B*. The fit for sample *A* is shown in Fig. 8.

Slightly different values for *J* were obtained when an al-

ternative method of correcting for the paramagnetic ions, based on the Brillouin function and the Curie law, was used.[28] The values of J for samples A and B obtained with this alternative correction were 0.1–0.2 cm^{-1} lower in magnitude.

All the J values from the susceptibility are slightly lower in magnitude than the average value $J=-8.4\ cm^{-1}$ from the first two MST's. The differences, however, are comparable to the combined experimental uncertainties. In principle, the MST method is more direct, and therefore more accurate.

ACKNOWLEDGMENTS

We are grateful to R. B. Frankel for crucial advice. The work at Boston College was supported by NIH grant No. GM38275.

[1] R. L. Carlin, *Magnetochemistry* (Springer, Berlin, 1986).
[2] W. E. Hartfield, in *Theory and Applications of Molecular Paramagnetism*, edited by E. A. Boudreaux and L. N. Mulay (Wiley, New York, 1976).
[3] O. Kahn, *Molecular Magnetism* (VCH, New York, 1993).
[4] E. Sinn, Coord. Chem. Rev. **5**, 313 (1970); K. S. Murray, *ibid.* **12**, 1 (1974).
[5] R. D. Cannon and R. P. White, Prog. Inorg. Chem. **36**, 195 (1988).
[6] H. U. Güdel and A. Furrer, Mol. Phys. **33**, 1335 (1977); H. U. Güdel, A. Stebler, and A. Furrer, Inorg. Chem. **18**, 1021 (1979).
[7] T. M. Giebultowicz, J. J. Rhyne, J. K. Furdyna, and P. Klosowski, J. Appl. Phys. **67**, 5096 (1990).
[8] Y. Shapira, J. Appl. Phys. **67**, 5090 (1990).
[9] S. Foner, Y. Shapira, D. Heiman, P. Becla, R. Kershaw, K. Dwight, and A. Wold, Phys. Rev. B **39**, 11 793 (1989).
[10] V. Bindilatti, N. F. Oliveira, Jr., Y. Shapira, G. H. McCabe, M. T. Liu, S. Isber, S. Charar, M. Averous, E. J. McNiff, Jr., and Z. Golacki, Phys. Rev. B **53**, 5472 (1996).
[11] M. T. Liu, Y. Shapira, E. ter Haar, V. Bindilatti, and E. J. McNiff, Jr., Phys. Rev. B **54**, 6457 (1996).
[12] K. L. Taft, C. D. Delfs, G. C. Papaefthymiou, S. Foner, D. Gatteschi, and S. J. Lippard, J. Am. Chem. Soc. **116**, 823 (1994).
[13] A. Ganeschi, A. Cornia, A. C. Fabretti, S. Foner, D. Gatteschi, R. Grandi, and L. Schenetti, Chem.-Eur. J. **2**, 1379 (1996).
[14] M. Gerloch and F. E. Mabbs, J. Chem. Soc. A **1967**, 1900.
[15] M. Gerloch, J. Lewis, F. E. Mabbs, and A. Richards, J. Chem. Soc. A **1968**, 112.
[16] W. M. Reiff, G. J. Long, and W. A. Baker, Jr., J. Am. Chem. Soc. **90**, 6347 (1968).
[17] R. Lechan, C. Nicolini, C. R. Abeledo, and R. B. Frankel, J. Chem. Phys. **59**, 3138 (1973).
[18] M. Górska, J. R. Anderson, G. Kido, S. M. Green, and Z. Golacki, Phys. Rev. B **45**, 11 702 (1992); G. Bastard and C. Lewinger, J. Phys. C **13**, 1469 (1980).
[19] V. Bindilatti, T. Q. Vu, and Y. Shapira, Solid State Commun. **77**, 423 (1991).
[20] F. Varret, Y. Allain, and A. Miedan-Gros, Solid State Commun. **14**, 17 (1974); F. Varret, J. Phys. Chem. Solids **37**, 257 (1976).
[21] The structure was solved by direct methods and refined by full-matrix least-squares methods on F^2 with statistical weighting, anisotropic displacement parameters for all nonhydrogen atoms, and constrained isotropic H atoms to give $R_1=\{\Sigma[w(F_o^2-F_c^2)^2]/\Sigma[w(F_o^2)^2]\}^{1/2}=0.041$ on all data, conventional $R_1=0.052$ on $F_o^2>2\sigma F_o^2$, goodness of fit $S=1.094$ for all F^2 values and 1046 refined parameters. Programs employed: Siemens SMART and SAINT control and integration software (Siemens Analytical x-ray Instruments, Inc.), and Siemens SHELXTL-PLUS structure solution and refinement software (Siemens Industrial Automation Inc.).
[22] W. P. Wolf, Phys. Rev. **115**, 1196 (1959).
[23] I. M. Khalatnikov, *An Introduction to the Theory of Superfluidity* (Benjamin, New York, 1965); see also W. A. Little, Can. J. Phys. **37**, 334 (1959).
[24] N. S. Snyder, Cryogenics **10**, 89 (1970).
[25] Only the acoustic modes of lattice vibrations contribute to the lattice specific heat at low temperatures, so that a model with 1 atom per cell is adequate.
[26] W. M. Reiff, W. A. Baker, Jr., and N. E. Erickson, J. Am. Chem. Soc. **90**, 4794 (1968).
[27] J. A. Gaj, R. Planel, and G. Fishman, Solid State Commun. **29**, 435 (1979).
[28] The magnetization of the paramagnetic ions was assumed to follow the Brillouin function, with the actual temperature T. As a consequence, the low-field susceptibility obeyed the Curie law. The fits of the 2 K magnetization were carried out using Brillouin functions for various assumed values for the spin S of the paramagnetic ions. To obtain good fits it was necessary to adjust the g factor, in addition to M_{para}. The values for M_{para} were practically independent of S, and were close to those obtained from the procedure which used the modified Brillouin function of Ref. 27. Although the results for the g values did depend on S, the calculated susceptibility of the paramagnetic ions was practically independent of S.